

## ARTICLE OPEN

## Simultaneous production and functionalization of hexagonal boron nitride nanosheets by solvent-free mechanical exfoliation for superlubricant water-based lubricant additives

Lulu An<sup>1,2</sup>, Yuanlie Yu<sup>1,2</sup>, Changning Bai<sup>1,2</sup>, Yongqing Bai<sup>1,2</sup>, Bin Zhang<sup>1,2</sup>, Kaixiong Gao<sup>1,2</sup>, Xinbo Wang<sup>3,4</sup>, Zhiping Lai<sup>3,4</sup> and Junyan Zhang<sup>1,2</sup>

Hexagonal boron nitride nanosheets (*h*-BNNs), with a crystal lattice structure similar to graphene by over 98%, exhibit good lubrication properties as lubricant additives. However, the poor dispersibility in solvents has limited their wide practical applications as lubricant additives. In the present report, water dispersible Pebax functionalized *h*-BNNs (Pebax-BNNs) have been prepared through a one-step solvent-free mechanical exfoliation process which relies on a simple exfoliation of *h*-BN layers by shearing force in molten Pebax at 200 °C. In this process, Pebax molecules can synchronously react with the dangling bonds formed during the exfoliation process to achieve in situ functionalization of *h*-BNNs. The reciprocating friction tests demonstrate that the as-obtained Pebax-BNNs possess excellent antifriction and antiwear performance as water-based lubricant additive with a low concentration of 0.3 mg/mL under atmospheric condition. The friction coefficients can be <0.01, achieving superlubrication. Further systematical investigations on the wear traces, wear debris, and counter balls propose a “dispersion-compensation-filling repairment” friction mechanism. All these results demonstrate that *h*-BNNs can achieve superlubrication as water-based lubricant additives via facile surface modification, making them very promising candidates as lubricant additives in practical applications.

npj 2D Materials and Applications (2019)3:28; <https://doi.org/10.1038/s41699-019-0111-9>

## INTRODUCTION

Friction and wear remain the primary modes of mechanical energy dissipation in many mechanical, electromechanical, and biological systems, resulting in unwanted wastage of resources and energy<sup>1</sup> as well as 80% of machinery component failure.<sup>2</sup> It is estimated that the wastage of resource has grown to over 6% of the Gross Natural Product, making the investigation of friction and wear becomes extremely significant.<sup>3</sup> Moreover, the needs of “green” lubricant are rising because of the increasing concerns on environmental protection. The development of environment-friendly lubricants has thus become a global requirement.<sup>4,5</sup> Currently, oil lubrication has been regarded as one of the most common and widely used antifriction and antiwear ways due to its good lubricating effect. However, most of the oil-based lubricants contain mineral oil, which could seriously pollute soil and water resources in case of spill or discharge. In this regard, development of environment-friendly lubricants for practical application with good antifriction and antiwear performance is of great importance. Recently, water-based lubricants have attracted increasing attention due to their outstanding properties, such as high fire resistance and excellent environmental friendliness.<sup>6,7</sup> As a result, it is becoming significant to explore and develop novel water-based lubricants with good antifriction and antiwear performance.

Hexagonal boron nitride nanosheets (*h*-BNNs) are one of typical two-dimensional materials and show <2% crystal lattice

mismatch with graphene.<sup>8–10</sup> Consequently, *h*-BNNs share many common properties with graphene, such as outstanding mechanical strength, good optical property, and high thermal conductivity.<sup>11,12</sup> However, *h*-BNNs also have higher oxidation resistance and better chemical stability which are different from graphene,<sup>13,14</sup> making them promising in some harsh environment applications. Besides, the lamellar structure of *h*-BNNs which is also entirely assembled by means of weak van der Waals forces is similar to those of graphene and molybdenum disulfide.<sup>15,16</sup> This structure makes *h*-BNNs very attractive lubricant additives as graphene and molybdenum disulfide. More importantly, *h*-BN nanomaterials have excellent biocompatibility and have also been widely used as food packaging materials and cosmetic additives,<sup>17–19</sup> which implies that *h*-BN nanomaterials will not damage the living environment of human, animals, and plants in case of spill or discharge. Based on the above mentioned discussion, it is predictable that *h*-BNNs would be very promising candidate as “green” lubricant additive in practical applications.

Unfortunately, compared with graphene/graphene oxides, the utilization of *h*-BN nanomaterials as lubricant additives is much more difficult because of their poor dispersibility of in either water or lubricant oil.<sup>20</sup> Therefore, many efforts have been made to improve the dispersibility of *h*-BN nanomaterials in water/lubricant oil. For example, Chen et al. have tailored the size of *h*-BNNs by an optimized wet ball milling process with benzyl benzoate as a

<sup>1</sup>R&D Center of Lubricating and Protecting Materials, Lanzhou Institute of Chemical Physics, Chinese Academy of Sciences, 730000 Lanzhou, People's Republic of China; <sup>2</sup>Center of Materials Science and Optoelectronics Engineering, University of Chinese Academy of Sciences, 100049 Beijing, People's Republic of China; <sup>3</sup>School of Environmental Science and Engineering, Shandong University, 72 Binhai Road, Jimo District, 266237 Qingdao, Shandong, People's Republic of China and <sup>4</sup>Advanced Membrane and Porous Materials Center, Division of Chemical and Life Science and Engineering, King Abdullah University of Science and Technology, Thuwal 23955-6900, Saudi Arabia

Correspondence: Yuanlie Yu ([yuanliehl@licp.cas.cn](mailto:yuanliehl@licp.cas.cn)) or Junyan Zhang ([zhangjunyan@licp.cas.cn](mailto:zhangjunyan@licp.cas.cn))

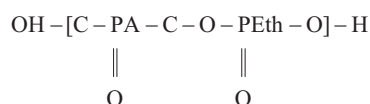
These authors contributed equally: Lulu An, Yuanlie Yu

Received: 9 April 2019 Accepted: 30 June 2019

Published online: 26 July 2019

milling agent.<sup>21</sup> These tailored *h*-BNNSs show good lubrication properties as base oil additives, which can greatly reduce the friction coefficients and wear rate of friction balls.<sup>22</sup> Khatri et al. have grafted octadecyltriethoxysilane onto the basal plane defects and edge sites of *h*-BN nanoplatelets to obtain octadecyltriethoxysilane-functionalized *h*-BN nanoplatelets (*h*-BNNSs-ODTESs) through chemical grafting process.<sup>20</sup> These *h*-BNNSs-ODTESs exhibit long-term dispersion stability in synthetic polyol ester lube base oil due to the van der Waals interaction between the octadecyl chains of *h*-BNNSs-ODTESs and alkyl functionalities of polyol ester.<sup>20</sup> The good dispersibility enables the *h*-BNNSs-ODTESs good lubricant properties as an additive that can significantly reduce both the friction coefficients and wear rates of steel disks. Obviously, it is effective to improve the dispersibility of *h*-BN nanomaterials in solvent with the assistance of surfactants or organic functionalization, so as to boost their lubricant properties. However, the friction coefficients with *h*-BN nanomaterials as lubricant additives are high, which are generally above 0.08. Therefore, it is vital to further decrease the friction coefficients and thus improve the antiwear performance of *h*-BN nanomaterial/water-based lubricants for practical applications.

Pebax comprises of rigid polyamide blocks and soft polyether blocks as illustrated in the following chemical formula:



This unique structure makes Pebax simultaneously possess good toughness associated with that of polyamides and high flexibility/elasticity resulted from polyethers. As a result, Pebax exhibits many excellent properties between the rigidity and flexibility, such as high elastic recovery, good flexibility, and excellent processing performance.<sup>23</sup> In addition, Pebax is also a bio-based material, which has been widely used in medicine and medical instruments.<sup>24,25</sup> Therefore, Pebax is selected to functionalize the *h*-BNNSs in the current report since the introduction of Pebax can combine the excellent properties of Pebax and *h*-BNNSs, thus giving *h*-BNNSs excellent lubrication performance. Moreover, the excellent biocompatibility of Pebax and *h*-BNNSs would also make the Pebax-BNNSs be excellent environment-friendly lubricant additives. Here, the fabrication of Pebax functionalized *h*-BNNSs (Pebax-BNNSs) involves solvent-free mechanical exfoliation of commercial *h*-BN powders in molten Pebax at 200 °C carried out in an Xplore (MC 15) micro compounder as shown in Fig. 1. Pebax molecules will synchronously react with the unsaturated bonds generated during the exfoliation process to achieve in situ functionalization of *h*-BNNSs. The morphology and composition of the as-obtained Pebax-BNNSs were characterized by complementary imaging and spectroscopic technologies including field emission scanning electronic microscopy (FESEM), transmission electron microscopy

(TEM), high resolution transmission electron microscopy (HRTEM), energy dispersive X-ray spectroscopy (EDX), atomic force microscopy (AFM), Fourier transform infrared spectroscopy (FTIR), Raman, thermogravimetric analysis (TGA), ultraviolet absorption spectrum (UV-vis), and X-ray photoelectron spectroscopy (XPS). The Pebax-BNNSs/water “green” lubricant was prepared by simply dispersing the as-obtained Pebax-BNNSs into water under ultrasonication. The tribological properties were systematically investigated by measuring the friction coefficients and wear rates with the Pebax-BNNSs/water dispersions as lubricants under atmosphere conditions. Furthermore, the lubrication mechanism is proposed on the basis of the thorough characterization of the wear debris and worn surfaces of substrates and counter balls.

## RESULTS

### Characterization of the Pebax-BNNSs

The FESEM image of the original *h*-BN powders (Fig. S1a) shows microplate morphology with smooth edges and large lateral sizes ranging from several to tens of micrometers. After mechanical exfoliation by ultrasonication in water, the thickness and lateral size of *h*-BN are both obviously reduced (Fig. S1b). The preparation of the Pebax-BNNSs was performed through a solvent-free mechanical exfoliation process with commercial *h*-BN powders and Pebax 1657 as precursors as illustrated in Fig. 1. Figure 2a, b shows the low- and high-magnification FESEM images of *h*-BNNSs exfoliated by micro compounder with the assistance of Pebax at 200 °C. It can be seen clearly that a large number of nanosheets are randomly distributed on the substrate (Fig. 2a), which is even more obvious when the image is magnified as demonstrated in Fig. 2b. Moreover, the size and thickness of the products are greatly reduced compared with those of original *h*-BN powders with the lateral size from tens to hundreds of nanometers (Fig. S1). The microstructure of the as-obtained products was further characterized by TEM, EDX, and AFM analysis as shown in Fig. 2c–e. As can be seen from Fig. 2c, the as-obtained products are similar to graphene that the edges are apt to be folded. Figure 2d depicts the HRTEM image collected from the folded edge of the as-obtained products marked in Fig. 2c, showing that the *h*-BNNS is consisted of four layers. The lattice distance calculated between adjacent layers is about 0.34 nm (inset in Fig. 2d), which is consistent with that of typical (002) crystal plane of *h*-BN.<sup>26</sup> In addition, the morphologies of the *h*-BNNSs are irregularly and stacked together. The degree of transparency is indicative of the number of stacked layers that the thinner Pebax-BNNSs appearing lighter in color (Fig. 2c). The selected area electron diffraction (SAED) pattern inserted in Fig. 2c reveals the typical sixfold symmetry patterns of *h*-BN, indicating that the intrinsic lattice structure of *h*-BN is kept well after mechanical exfoliation and functionalization. The EDX spectrum of the as-obtained products (the inset in the upper part of Fig. 2c) demonstrates that the

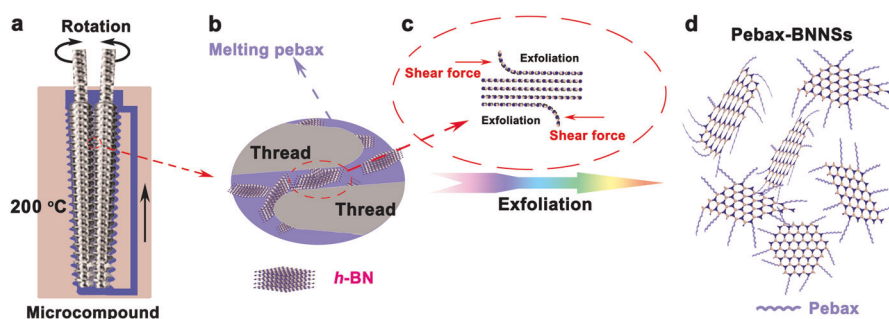


**Fig. 1** Schematic illustration for the exfoliation and dispersion of the Pebax-BNNSs. **a** The chamber for the exfoliation and in situ functionalization of *h*-BNNSs. **b, c** The exfoliation and in situ functionalization process of *h*-BNNSs. **d** The as-obtained Pebax-BNNSs. The Pebax molecules will randomly react with the dangling bonds formed during the mechanical exfoliation process

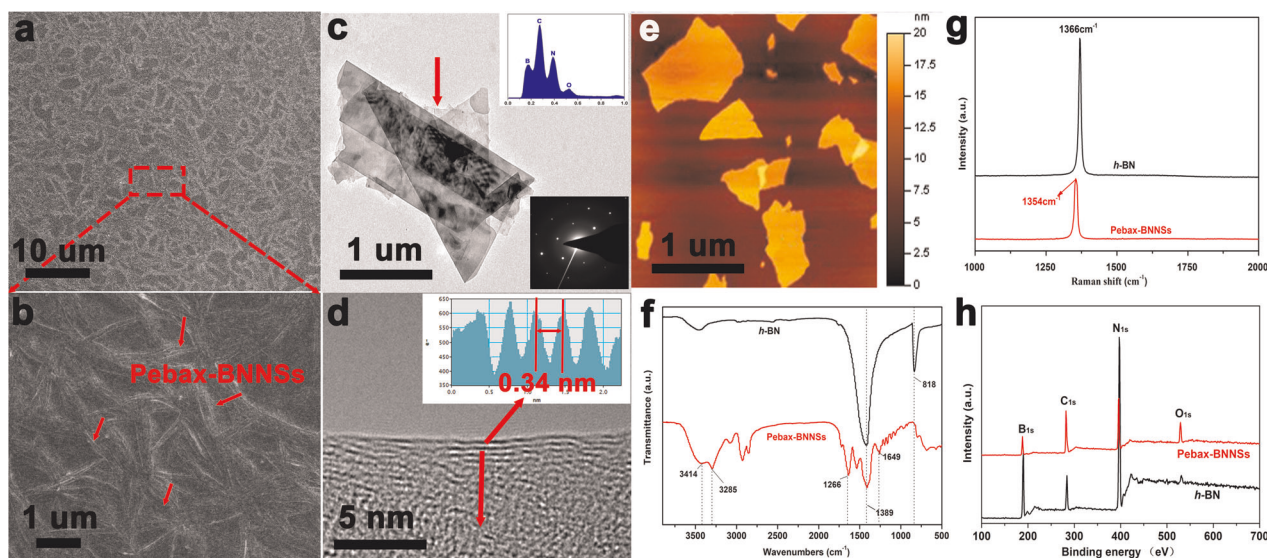


**Fig. 2** Nanostructure and characterization of the Pebax-BNNSs. **a** The low-magnification and **b** high-magnification FESEM images of the Pebax-BNNSs randomly distributed on the substrates. **c** The TEM image of the Pebax-BNNSs. Insets are the corresponding EDS spectrum and SAED pattern of the Pebax-BNNSs. **d** The HRTEM image of a single Pebax-BNNS with five layers. Inset is the corresponding distance profile of the area marked with the red line in **d**, showing a crystal spacing of 0.34 nm. **e** The AFM image shows that some Pebax-BNNSs randomly distribute on the substrates. The FTIR spectra (**f**), Raman spectra (**g**), and XPS spectra (**h**) of original *h*-BN and the as-obtained Pebax-BNNSs

products are composed of B, N, C, and O elements. This high content of C and O implies that Pebax has been introduced onto *h*-BNNSs by the mechanical exfoliation process. Figure 2e shows the AFM image in which several thin sheets can be clearly observed and distributed on the substrate. The average thickness of the as-obtained nanosheets is between 4 and 12 nm according to the statistics analysis of a large number of nanosheets (Fig. S2).

The Raman spectrum (Fig. 2g) of the original *h*-BN shows a band at  $1366\text{ cm}^{-1}$ , extremely closing to  $1365.8\text{ cm}^{-1}$  for typical *h*-BN, which can be attributed to the  $E_{2g}$  vibration mode of *h*-BN.<sup>27,28</sup> Different from the original *h*-BN, a slight redshift of  $12\text{ cm}^{-1}$  can be observed in the Raman spectrum of the as-obtained products. This result suggests that *h*-BN has been exfoliated to a few layered nanosheet predominant products since this feature can reduce the interlayer interactions and shorten the B–N bonds.<sup>29</sup> Another reason may be that the exfoliated *h*-BNNSs have been functionalized by Pebax, and the introduction of Pebax molecules cause the weakness and redshift of the Raman spectrum. In order to further validate whether there are Pebax molecules anchored on *h*-BNNSs, FTIR, and XPS were employed. As shown in Fig. 2f, the FTIR spectrum provides that the original *h*-BN has a strong and sharp absorption peak at  $818\text{ cm}^{-1}$  attributing to the out-of-plane B–N–B bending mode, and a very broad and strong vibration peak centered at  $1389\text{ cm}^{-1}$  ascribing to the in-plane B–N stretching mode.<sup>30,31</sup> Compared with the FTIR spectrum of original *h*-BN, several additional peaks can be observed in the FTIR spectrum of the as-obtained products. The peak at  $3285\text{ cm}^{-1}$  can be assigned to the N–H stretching vibration, while the other one at  $3415\text{ cm}^{-1}$  originates from O–H stretching vibration. Moreover, the peaks at 1266 and  $2750\text{--}3000\text{ cm}^{-1}$  can be attributed to C–C, C–H symmetric and antisymmetric stretching vibrations.<sup>32</sup> The FTIR results indicate that Pebax has been successfully attached on *h*-BNNSs, which can be further verified by XPS analysis. The intensity ratios of  $C_{1s}/B_{1s}$ ,  $C_{1s}/N_{1s}$ ,  $O_{1s}/B_{1s}$ , and  $O_{1s}/N_{1s}$  of the as-obtained products are obviously increased compared with those of original *h*-BN, indicating the existence of Pebax (Fig. 2h). In addition, the  $C_{1s}$  peak in original *h*-BN is observed which is associated with the carbon resulting from the exposure of *h*-BNNSs to air or during the XPS sample preparation process.<sup>33</sup> Based on the above analysis, it can be concluded that the Pebax has been successfully

functionalized onto *h*-BNNSs to form the Pebax-BNNSs. The content of the Pebax in the Pebax-BNNSs can be estimated by the TGA analysis (Fig. S3). Comparing the representative TGA trace of the Pebax-BNNSs with that of pure *h*-BNNSs, a mass loss of about 8.5% can be observed for the Pebax-BNNSs, while the *h*-BNNSs still remains a constant content up to  $550\text{ }^{\circ}\text{C}$ . The mass loss can be attributed to the oxidation of the Pebax attached on *h*-BNNSs,<sup>29</sup> indicating that the content of Pebax in the Pebax-BNNSs is about 8.5% in this case.

#### Dispersibility of the Pebax-BNNSs

The Pebax-BNNSs exhibit excellent dispersibility in water (Fig. S4). It is found that the Pebax-BNNS/water dispersion is very stable and has no precipitation after standing 30 days (Fig. S4a). In comparison, the *h*-BNNS/water dispersion begun to precipitate when it was prepared, and a distinct layer of the white precipitate can be found at the bottom after standing 30 days (Fig. S4a). Here, it is noteworthy that the Pebax-BNNS/water dispersion is white or beige, which is more suitable for the instruments that need to avoid dyeing contamination. For further demonstrating the stability of the Pebax-BNNSs in water, the UV-vis analysis for *h*-BNNS/water and Pebax-BNNS/water dispersions was performed (Fig. S4b and c). The results show that the absorbance of the Pebax-BNNS/water dispersion has no obvious change over a long time (Fig. S4c), demonstrating that the Pebax-BNNS/water dispersion is extremely stable and no aggregation or sedimentation occurs. However, the intensities of the UV-vis spectra of *h*-BNNS/water dispersion gradually decrease from the first day of standing (Fig. S4b), indicating the unstable dispersibility of pure *h*-BNNSs in water. Since the lubrication performance of *h*-BNNSs as lubricant additives is greatly limited by their dispersibility in water/organic solvents,<sup>8</sup> this improved dispersibility of the Pebax-BNNSs in water will ensure them excellent lubrication properties as lubricant additives.

#### The friction and wear performance of the Pebax-BNNSs as water-based lubricant additives

Figure 3 depicts the variation of the friction coefficients and wear rates of the substrates under different friction conditions with the

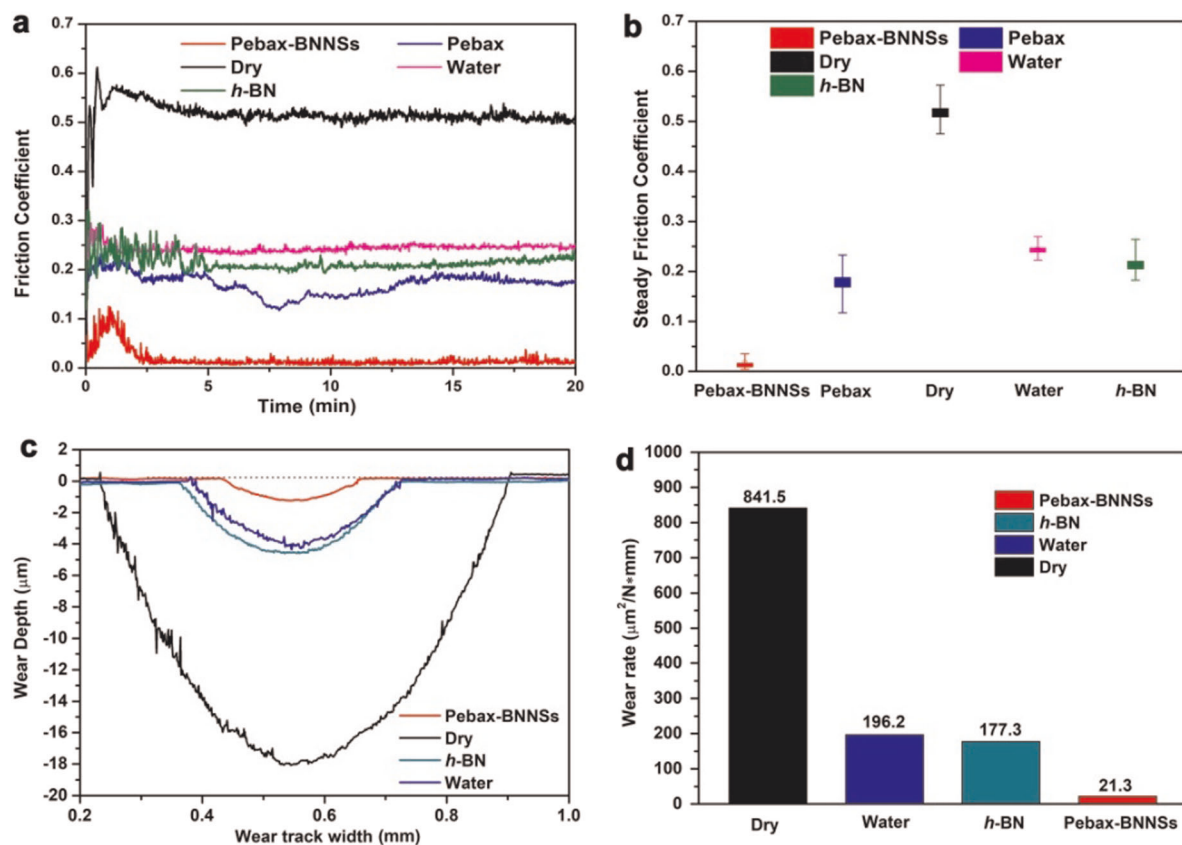


**Fig. 3** The friction and wear performance with different materials as lubricants. **a** The friction curves with different materials as lubricants. **b** The comparison of the friction coefficients with different materials as lubricants. **c** The wear scar profile and **d** corresponding wear rates with different materials as lubricants. The friction load is 2 N and speed is 3 cm/s

same friction load of 2 N and speed of 3 cm/s. It can be seen from Fig. 3a, b that the friction coefficients under dry friction condition are the highest which are in the range of 0.45–0.6. When the water or *h*-BN/water dispersion was added as lubricants, the friction coefficients will decrease to the range of 0.18–0.25 (Fig. 3a, b). The steady-state friction coefficients with water as a lubricant are close to those with *h*-BN/water dispersion as a lubricant, and the former is a little higher reaching up to about 0.25 (Fig. 3a). When the Pebax/water solution was added as a lubricant, the friction coefficients further decrease and are in the range of 0.1–0.23 (Fig. 3a, b). However, the friction coefficients can significantly reduce to <0.01, reaching ultralow friction when the Pebax-BNNS/water dispersion was added as a lubricant (Fig. 3a, b). The lowest friction coefficients can reach ~0.003–0.009, achieving superlubrication (Fig. 3b). The wear tracks and wear rates under different friction conditions were also evaluated based on the analysis of three-dimensional contour chart. Figure 3c provides the wear track profiles of the substrates after reciprocating friction tests under different friction conditions. The depths of the wear scars are 18.3, 4.79, 4.33, and 1.42 μm for the different friction conditions under dry friction, with water, *h*-BN/water dispersion and Pebax-BNNS/water dispersion as lubricants, respectively. Correspondingly, the wear volumes are respectively 8415, 1962, 1773, and 213 μm<sup>3</sup>. Then, the wear rates under different friction conditions can be calculated according to the following equation (1):

$$W = V / (F * L) \quad (1)$$

where  $W$ ,  $F$ ,  $V$ , and  $L$ , respectively represent wear rate, positive pressure, wear volume, and slip distance. The wear rates under different friction conditions are shown in Fig. 3d, which are 841.5, 196.2, 177.3, and 21.3 μm<sup>3</sup>/(N mm) for different friction conditions

under dry friction, with water, *h*-BN/water dispersion and Pebax-BNNS/water dispersion as lubricants, respectively. Obviously, the wear rate with the Pebax-BNNS/water dispersion as a lubricant is much lower comparing with those of the other three friction conditions. In addition, it is worth noting that the typical variation law of friction coefficients can be observed from Fig. 3a, which can be divided into two states of running-in stage and steady-state stage except for the one under dry friction condition.<sup>34,35</sup> In the running-in stage, the initial friction decreases gradually, which indicates the transfer of the Pebax-BNNSs at the friction interface. Also, the stable dispersion of the Pebax-BNNSs in water ensures their continuously and timely supply between tribological interface.

It is well known that the tribological performance of a material depends on the way of the evaluation processes, such as the testing conditions and the moving modes of the frictional tester and the testing counterparts. Therefore, the tribological properties of the Pebax-BNNS/water dispersion under different loads and friction frequencies and with different balls as counterparts were evaluated. The loads show a great influence on the friction coefficients at the same frequency (4 Hz) (Fig. S5a and c), and the friction coefficients increase with the increment of loads for both silicon nitride (Si<sub>3</sub>N<sub>4</sub>) and alumina (Al<sub>2</sub>O<sub>3</sub>) counter balls. The friction coefficients with Si<sub>3</sub>N<sub>4</sub> ball as counterpart are higher than those with Al<sub>2</sub>O<sub>3</sub> ball as counterpart under dry friction condition (Fig. S5a and c). This may be caused by the higher surface roughness of Si<sub>3</sub>N<sub>4</sub> ball than that of Al<sub>2</sub>O<sub>3</sub> ball. In addition, it should be noted that both balls can achieve ultralow friction under the load of 2 N. On the contrary, the effect of friction frequency on the friction coefficients is very small (Fig. S5b and d). The friction coefficients are basically consistent in the steady-state

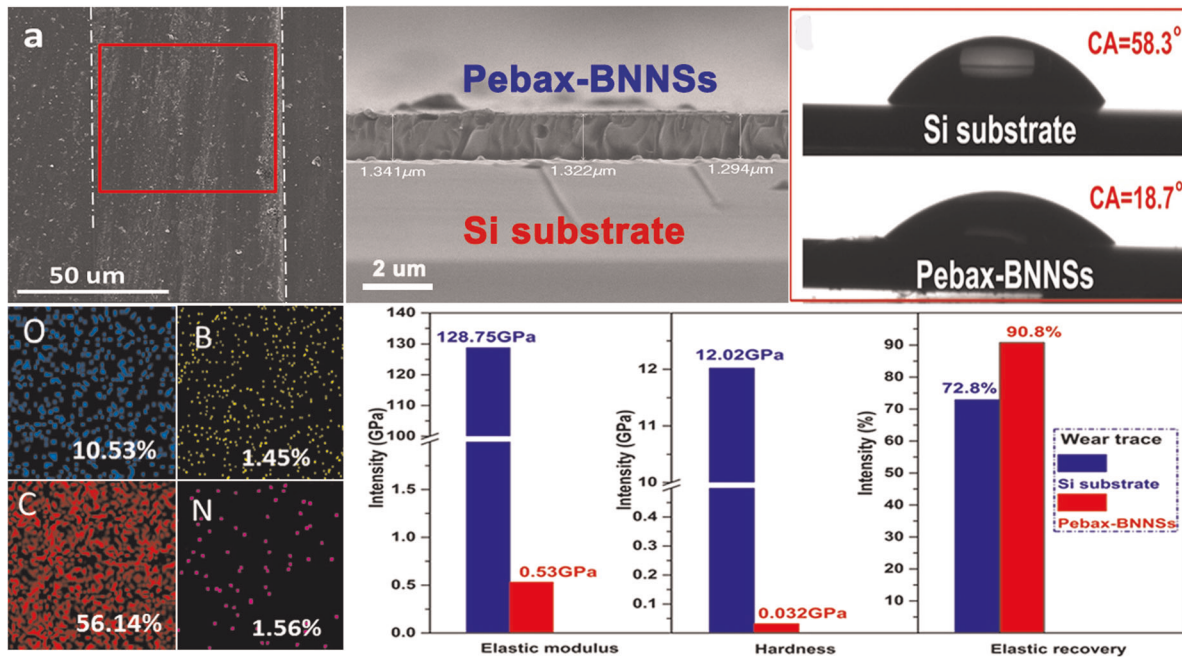


**Fig. 4** The characteristics of protective film to achieve superlubrication. **a** The FESEM image and corresponding element distribution diagram of the worn surface formed with the Pebax-BNNS/water dispersion as a lubricant. **b** The FESEM image of the worn surface cross-section formed with the Pebax-BNNS/water dispersion as a lubricant. **c** The photographs of water droplets on the surfaces of bare Si substrate with a contact angle (CA) of 58.31° and wear trace formed with the Pebax-BNNS/water dispersion as a lubricant with a CA of 18.7°, respectively. **d** The comparison of mechanical properties of the wear trace with and without the Pebax-BNNS/water dispersion as a lubricant

stage and are all in the superlubrication state for the friction with  $\text{Si}_3\text{N}_4$  ball as counterpart under the load of 2 N and frequencies from 1 to 8 Hz, respectively (Fig. S5b). Although the friction with  $\text{Al}_2\text{O}_3$  ball as counterpart can also enter into the superlubrication state under the same conditions, the friction coefficients are not stable (Fig. S5d). These results indicate that the superlubricity can be achieved for the Pebax-BNNS/water dispersion as water-based lubricant under certain friction conditions.

## DISCUSSION

The FESEM characterization was performed on the surfaces of the wear scars to explore the friction mechanism of the Pebax-BNNS/water dispersion as a lubricant. The wear track with a width of about 470 μm can be observed for the friction condition under dry friction, and a lot of wear debris accumulated on both sides of the track (Fig. S6a). However, compared with the wear track formed under dry friction, the wear tracks formed under the friction conditions with *h*-BN/water and Pebax-BNNS/water dispersions as lubricants are relatively narrow (~190 μm), and the whole friction surfaces are relatively smooth without obvious debris accumulation (Fig. S6d and g). In particular, there is barely no wear scar for the friction condition with the Pebax-BNNS/water dispersion as a lubricant (Fig. S6g). The enlarged FESEM images (Fig. S6b, e and h) reveal that protective films are formed on the wear surfaces with *h*-BN/water (Fig. S6e) and Pebax-BNNS/water (Fig. S6h) dispersions as lubricants. Moreover, the wear surface with the Pebax-BNNS/water dispersion as a lubricant is flatter than that with *h*-BN/water dispersion as a lubricant. When dry friction occurs, the slightly adhesive wear happens on the substrate surface, resulting in the formation of fine abrasive dust on the worn surface. This abrasive dust can form a flocculent surface (Fig. S6c), leading to high and fluctuated friction coefficients. When the Pebax-BNNS/water dispersion is added as a lubricant, the Pebax-BNNSs will accumulate on the substrate surface to form a protective layer, thus reducing the adhesion wear. Besides, due to the layered structure of the Pebax-BNNSs, the van der Waals force between

the adjacent layers is liable to fracture, resulting in mechanical separation of the Pebax-BNNSs under slight shearing force.<sup>36</sup> This slight separation of *h*-BN layers could also lead to the decrease of the coefficients. However, although the friction protective film is also formed under the friction condition with *h*-BN/water dispersion as a lubricant, a large number of small particles can still be observed agglomerated on the wear surface. This is most likely caused by the poor dispersibility of pure *h*-BN in water, and these agglomerated particles will hinder the further decrease of the friction coefficients. But for the Pebax-BNNSs with excellent dispersibility in water cannot agglomerate during the friction process (Fig. S6h and i), thus reducing the friction and wear effectively. Here, the formation of this friction film can be regarded as a “dispersion-compensation-filling repairment” mechanism, which will be further discussed later.

In order to explore the specific information of the protective antifriction film, the surface of the wear track was scanned by elemental analysis. As shown in Fig. 4a, a large amount of silicon, B, N, C, and O elements respectively with contents of 30.32, 1.45, 1.56, 56.14, and 10.53% are detected. This result indicates that a smooth layer comprised of B, N, C, and O elements is formed on the silicon substrate. Chen et al. have proposed that the flatter the friction layer is, the higher the reduction of friction will be. In other words, the flatter and smoother the friction layer is, the higher the opportunity to achieve superlow friction will be.<sup>37</sup> The cross-section analysis on the above wear track reveals that a very smooth and compact protective antifriction film (Fig. 4b) is formed. The average thickness of this protective antifriction film calculated from three different positions is about 1.319 μm (Fig. 4b). This film is stable and well adheres on the friction surface, showing good shearing strength and bearing capacity. The above characteristics are fully consistent with the basic characteristics of solid lubrication film.<sup>38</sup> Therefore, the protective antifriction film formed in the friction pair can be regarded as a solid lubrication film which is beneficial to achieving the superlow friction. In addition, the water contact angles greatly decrease from 58.3° (Si substrate) to 18.7° due to the formation of the protective

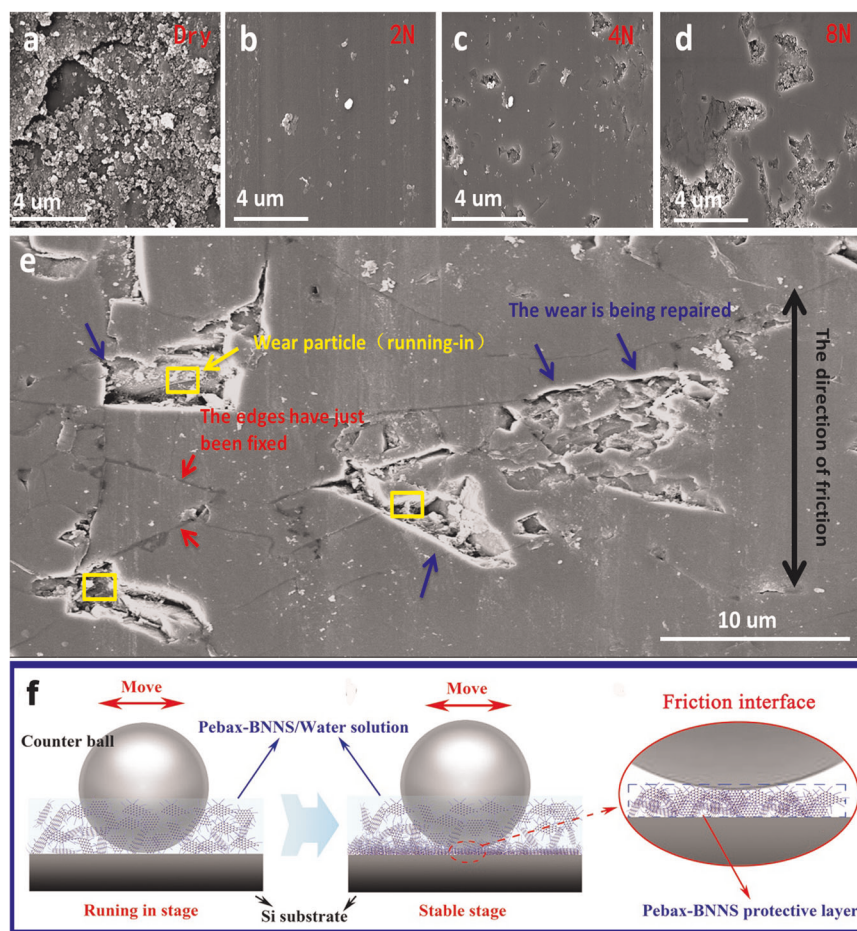


**Fig. 5** The FESEM images of worn surfaces under different loads. **a** The FESEM image of a wear trace with water as a lubricant. Many particles can be found in the wear trace. **b–d** The FESEM images of the wear traces with the Pebax-BNNS/water dispersion as lubricants under test conditions with loads of 2, 4, and 8 N, respectively. Only a small amount of particles can be found in the wear traces. **e** The high-magnification FESEM image of a wear trace with incomplete protective film. **f** The schematic illustration for the formation of the protective film during the friction process

antifriction film since the existence of hydroxyl hydrophilic groups in the Pebax molecules (Fig. 4c). The existence of the protective antifriction film can significantly improve the infiltration capacity of the substrate, making the sliding interface more hydrophilic.<sup>37</sup>

Our previous work has demonstrated that the high elasticity of a film is beneficial to the superlow friction.<sup>39,40</sup> Figure 4d and Fig. S7 show the mechanical properties of the wear tracks with and without the Pebax-BNNS/water dispersion as a lubricant. Clearly, the hardness (0.032 GPa) and elastic modulus (0.53 GPa) of the wear track after formation of the solid lubrication film have been significantly reduced compared with those (hardness: 12.02 GPa, and elastic modulus: 128.75 GPa) of the wear track without the solid lubrication film (Fig. 4d). It is well known that the elastic modulus is an indicator to evaluate the difficulty of material deformation, and the larger the elastic modulus is, the smaller the elastic deformation of a material will be. Therefore, the elastic modulus and hardness of the solid lubrication film formed by Pebax-BNNSs are significantly reduced, which means that the elasticity is significantly increased. The changes of the elastic recovery curves (Fig. S7) and elastic recovery values (Fig. 4d, increased from 72.8 to 90.8%) with and without the solid lubrication film can also demonstrate the increase of the elasticity of the solid lubrication film. Therefore, combining with the above analysis, the film that can achieve superlubrication is a solid lubrication film with certain elasticity.

Lee et al. have demonstrated that the layered structure and flexibility of composite nanosheets can facilitate mending and polishing effect.<sup>41</sup> As discussed above, the friction coefficients are dependent on the loads with  $\text{Si}_3\text{N}_4$  ball as friction counterpart, which may be greatly dominated by the solid lubrication film. Therefore, the wear tracks formed under different loads of 2, 4, and 8 N after 30 min of friction were investigated in detail. The wear track formed only under the dry friction condition with a load of 2 N shows a large number of wear particles randomly distributed on the wear surface after 30 min friction test (Fig. 5a). Inversely, when the Pebax-BNNS/water dispersion was used as a lubricant, the amount of the wear particles significantly reduces, and a large amount of “holes” appear with the increase of the loads from 2 to 8 N as demonstrated in Fig. 5b–d. The size of the concave pits becomes larger when the load increases to 8 N (Fig. 5d). On the contrary, the solid lubrication film formed under the load of 2 N is relatively smooth and complete, and no “holes” are found (Fig. 5b). To further evaluate the solid lubrication film, a representative FESEM image focused on the “holes” formed under the load of 8 N is displayed in Fig. 5e. This image can well explain the formation of the superlubrication solid film. As shown in Fig. 5e, the black arrow represents the direction of the reciprocating friction, and the “holes” will form as marked with yellow arrows and rectangles during the running-in stage. With friction time increases, the dispersed Pebax-BNNSs could enter into these “holes” and “repair” them to form the superlubrication solid film.

The blue arrows in Fig. 5e represent the “holes” which are being repaired, and the red arrows mark the edge traces of the repaired “holes” during the friction process. Here, actually, the “holes” mentioned above are not really holes formed by collapse or destruction of Si substrates, rather than “repairing pits” of uncompleted solid lubrication film (Fig. S8). It should be emphasized that, unlike simple solid lubrication (solid powders, coating films or other materials are used to prevent the friction surfaces in contact and yield the reduction of friction and wear),<sup>42</sup> the Pebax-BNNSs used as a lubricant additives in current experiment will twine around each other in the assistance of Pebax molecules to form a solid film near the wear part through a series of friction processes (Fig. 5f).

In addition, the wear of Si<sub>3</sub>N<sub>4</sub> ball-silicon friction pair in the running-in stage is generally dominated by adhesion and furrow effect. Due to the formation of a series of defects mentioned in the simple adhesion theory, Wen and Huang have proposed a more complete revised adhesion friction theory (2):<sup>43</sup>

$$f = \frac{\tau_f}{\sigma_s} \quad (2)$$

where  $\tau_f$  is the shear strength limitation of the soft material film, and  $\sigma_s$  is the yield stress limitation of the hard material film. In fact, in the general sliding process, due to the presence of tangential force, the actual contact area and deformation conditions of the contact point depend on the positive pressure generated by the synergistic effect of load and shearing force produced by the tangential force. Therefore, the revised adhesion friction theory is very suitable for the actual situation. The revised adhesion friction theory indicates that a thin flexible material-based layer is required to cover on the hard metal surface to reduce the friction coefficients.<sup>44,45</sup> In our work, as the friction process continues, an antifriction Pebax-BNNSs film with certain elasticity is formed on the friction surface, and the sliding on this flexible antifriction Pebax-BNNSs film will maintain a very low shearing strength. In addition, because the thickness of the antifriction Pebax-BNNSs film is only about 1.3  $\mu\text{m}$ , the actual contact area will be determined by the limited pressure, which means that the actual contact area is very small. Therefore, a thin antifriction Pebax-BNNSs film with certain elasticity can reduce the friction coefficients.

Based on the above analysis, the following is a systematic description for the formation of the solid lubrication film (Fig. 5f): (1) In the running-in stage, a small amount of wear particles are produced due to the adhesion and furrow effects on silicon substrate; (2) As the friction process continues, dispersed Pebax-BNNSs will gradually enter into the friction interface and twine around each other to form the antifriction film near the wear part. During this process, the small amount of wear particles will also be gradually covered; (3) The Pebax-BNNSs and coated particles will gradually stack due to the shearing force to form the antifriction solid film. During this process, the “repairing pits” can be formed in places where the stack is not completely flattened. As the friction continues, these “repairing pits” will be gradually filled and form a relatively complete antifriction solid film. Therefore, superlubrication friction film is generated, which can effectively reduce the friction and wear. The subsequent friction process will continue in the state of ultralow friction with the friction coefficient of 0.003. This result well supports the proposed superlubrication mechanism of “dispersion-compensation-filling repairment”.

Furthermore, Raman and TEM analysis were conducted on the friction tracks, friction spots, and debris formed on the counterpart Si<sub>3</sub>N<sub>4</sub> ball for further demonstrating the super-lubrication mechanism. It is well known that the typical diamond-like carbon (DLC) films have macroscopic super-lubrication properties since the DLC is a kind of amorphous carbon (a-C) composed of  $sp^2$  and  $sp^3$  carbon atom-based disorderly network. One of the mechanisms to

explain this super-lubrication property is that the surface of a-C:H film has enormous deactivation bonds deactivated by hydrogen.<sup>2,22,46,47</sup> The existence of these C–H bonds can greatly reducing the friction coefficients. Here, this super-lubrication mechanism is also applicable to explain the case in current report. The Raman spectra (Fig. S9) of the friction scar on different sites show weak peaks located at about 1360  $\text{cm}^{-1}$  that can be assigned to the characteristic peak of *h*-BN, while the G (1600  $\text{cm}^{-1}$ ) and G' (2700  $\text{cm}^{-1}$ ) peaks are typical characteristic peaks of carbon-based materials. This result indicates that the as-formed solid friction film also contains carbon which is formed by Pebax (Fig. S9a). The values of  $I_{D'/G}$  obtained from different sites show little change, indicating that in the as-formed carbon film is rich in  $sp^2$ -C phase and the structure is mainly same. Kondyurin et al. have studied the surface carbonization and oxidation processes of different types of polyamide-polyether polymers, and demonstrated that graphite and diamond-like structures will form in the physically modified Pebax material surface.<sup>48</sup> Moreover, in Raman spectrum, the peak at about 2800  $\text{cm}^{-1}$  corresponding to C–H bonds can also be clearly observed. Hayashi et al. have found that the hydrogen atoms are considered from the local high-stressed C–H asperities, making C atoms re-hybridized into  $sp^2$ -C.<sup>32</sup> The formation of the solid antifriction film containing carbon and C–H bonds which is similar to a-C:H film is beneficial to reducing the friction. In addition, the peaks in the range of 800–1100  $\text{cm}^{-1}$  originate from  $\beta$ -Si<sub>3</sub>N<sub>4</sub> that peeled off from the counterpart ball, while the peak at 523  $\text{cm}^{-1}$  can be attributed to the silicon substrate. Clearly, the peaks attributed to the silicon can be only observed at site-5 (Fig. S9b), indicating that there is very little wear and tear on the silicon substrate and therefore no significant enrichment on the transfer film. Consistent with the Raman spectra of the wear track in the substrate, the Raman peaks at 1300, 1600, 2700, and 2800  $\text{cm}^{-1}$ , respectively, corresponding to D, G, G', and C–H bands are also observed for the wear scar on the friction counter ball (Fig. S9b). This result implies that  $sp^2$ -C transfer film containing C–H bonds has also formed on the friction counter ball during the friction process. This  $sp^2$ -C transfer film containing C–H bonds is mainly amorphous structure which can be verified by the TEM and SAED analysis (Fig. S10). The layered structure with a typical spacing of 0.34 nm enwrapped by amorphous structure can be clearly observed in the debris. The layered structure can be attributed to the Pebax-BNNSs (Fig. S10b), while the amorphous structure is from amorphous carbon (Fig. S10c). The SAED pattern (inserted in Fig. S10a) shows a very symmetrical sixfold structure, which means that the crystal structure of *h*-BN remains intact in the friction process. The retaining of the crystal structure of *h*-BN can provide a continuous superlow shearing force for obtaining superlow friction coefficients.

However, under different friction conditions, the superlubrication mechanisms of Pebax-BNNS/water lubricants have their complexity and diversity, which are caused by the synergistic effect of many factors. Therefore, a further investigation from multiple perspectives is needed in future. In conclusion, the Pebax-BNNSs as water dispersible lubricant additives have excellent antifriction and antiwear performance and show great potential in many aspects.

In summary, the Pebax-BNNSs can be prepared via a simple one-step solvent-free mechanical exfoliation process with commercial *h*-BN powders and Pebax as precursors. The as-obtained Pebax-BNNSs exhibit excellent dispersibility in water that can be used as water-based lubricant additives. The reciprocating friction tests show that the friction coefficients are dependent on the loads, and the lowest friction coefficient of about 0.003 can be obtained when the load is 2 N with Si<sub>3</sub>N<sub>4</sub> ball as a counterpart. The investigation on the wear debris and wear scars suggests that the solid antifriction polymerization film is formed by the Pebax-BNNSs through a “dispersion-compensation-filling repairment”

mechanism. This solid friction polymerization film can prevent friction and wear. Moreover, the Pebax-BNNSs can well maintain a complete layered structure during the friction process to ensure the continuous action of superlow shearing force, so as to achieve superlubrication. This result demonstrates that the as-obtained Pebax-BNNSs can be used as excellent water-based lubricant additives and achieve superlubricity. The excellent tribological performance combining with the outstanding properties of *h*-BNNSs makes them promising candidates as lubricant additives for practical applications.

## METHODS

### Preparation of the Pebax-BNNSs

The preparation of Pebax-BNNSs was performed through a solvent-free mechanical exfoliation process with commercial *h*-BN powders and Pebax 1657 as precursors as illustrated in Fig. 1. Typically, 13 g of Pebax 1657 powders was firstly added into the Xplore micro compounder which was preheated to 200 °C. When the Pebax 1657 powders were completely melted, 2 g of commercial *h*-BN powders was added for further mechanical exfoliation of 4 h. Then, the products were cooled down to room temperature naturally when the exfoliation process terminated. Finally, the Pebax/*h*-BN mixture was dissolved in water/ethanol (7/3 v/v) solution at 150 °C under magnetic stirring for subsequent separation.

### Separation of the Pebax-BNNSs

The products suspended in water/ethanol solution are composed of unexfoliated *h*-BN flakes, exfoliated few-layer Pebax-BNNSs and small *h*-BN particles. The unexfoliated large *h*-BN particles could be firstly separated out by centrifugation with a speed of 1000 rpm for 20 min. Subsequently, the supernatant was collected and centrifuged again with a high speed of 8000 rpm for another 20 min to remove the small particles. Next, the precipitates were collected and again uniformly dispersed in water/ethanol solution at 150 °C under magnetic stirring to completely remove the free Pebax 1657. Then, the suspensions were centrifuged at 3000 rpm for 20 min again, and the supernatant was collected. Finally, the Pebax-BNNSs can be obtained after centrifugation of the collected supernatant at 8000 rpm. In addition, the *h*-BNNSs prepared by ultrasonication process were used for comparison<sup>26</sup>.

### Materials characterization

The morphologies of *h*-BN, *h*-BNNSs, Pebax-BNNSs, wear debris, and wear scar were characterized by FESEM (JSM-6701F) and Tecnai-G2 F30 TEM (FEI, US), respectively. The Raman spectra were collected by a Raman spectrometer (LABRAM HR 800) at a wavelength of 600 nm (2.3 eV). The composition and bonding state of Pebax-BNNSs were analyzed by XPS (VG ESCALAB 210) with Al-K $\alpha$  (1486.5 eV) X-ray radiation. Surface topography images were obtained using an AFM (Agilent 5500) in tapping mode with a commercially available type-II MAC lever, of which the nominal force constant was 2.8 N/m. The UV-vis spectra were obtained by a UV-vis spectrophotometry (Cary 50) at 480 nm. FTIR of all samples was recorded using Nexus 870 with a resolution of 4 cm<sup>-1</sup>. The wear scar under different friction conditions were scanned and calculated by using a Micro-XAM 3D surface profiler (GBS Smart WLI, GER) based on scanning white light interferometry under different conditions. The mechanical properties of friction film were measured and analyzed by the TriboIndenter in situ nanomechanical test system (Ti 950).

### Friction and wear tests

The tribological performance was evaluated at room temperature (23 °C) on a friction and wear tester with a reciprocating ball-on-disc configuration selecting commercial Si<sub>3</sub>N<sub>4</sub> and Al<sub>2</sub>O<sub>3</sub> balls ( $\Phi = 6$  mm) as counterparts, which had been cleaned ultrasonically in acetone and methanol prior to each test. The silicon wafer N (100) was used as substrate, which was fixed on the testboard of the tester. The *h*-BN/water and Pebax-BNNS/water dispersions with concentration of 0.3 mg/mL were added as lubricants during the tribological performance tests. In comparison, the tribological performance under the conditions of dry friction and with water and Pebax/water as lubricants was also measured. The applied normal loads were selected to be 1, 2, 3, 4, 5, 6, 7, and 8 N, and the sliding frequencies

were 1, 2, 3, 4, 5, 6, 7, and 8 Hz, respectively. The reciprocating distance was 5 mm, and the testing time was set to be 30 min. All the friction tests were carried out at least three times to ensure the repeatability.

## DATA AVAILABILITY

All data related to the manuscript is available on request from the corresponding authors.

## ACKNOWLEDGEMENTS

This work was supported by the Foundation of Lanzhou Institute of Chemical Physics, the National Natural Science Foundation of China (51875550, 51527901, and U1737213), the Youth Innovation Promotion Association (2017459), and the Science and Technology Program of Gansu Province (18JR3RA380).

## AUTHOR CONTRIBUTIONS

Y.L.Y. and J.Y.Z. conceived and directed the project. L.L.A., Y.L.Y., and J.Y.Z. designed the experiments. L.L.A., Y.L.Y., and X.B.W. prepared the samples. L.L.A., Y.L.Y., and Y.Q. B. performed the materials characterization. All authors contributed to analysis of the data and discussions of results. Y.L.Y., L.L.A., and J.Y.Z. wrote the manuscript with input from all authors.

## ADDITIONAL INFORMATION

**Supplementary Information** accompanies the paper on the *npj 2D Materials and Applications* website (<https://doi.org/10.1038/s41699-019-0111-9>).

**Competing interests:** The authors declare no competing interests.

**Publisher's note:** Springer Nature remains neutral with regard to jurisdictional claims in published maps and institutional affiliations.

## REFERENCES

1. Songfeng, E. et al. Tribological characteristics of boron nitride nanosheets on silicon wafers obtained by the reaction of MgB<sub>2</sub> and NH<sub>3</sub>. *Surf. Coat. Technol.* **340**, 36–44 (2018).
2. Mo, Y. H., Tao, D. H., Wei, X. C. & Li, Q. H. Research on friction-coatings with activated ultra-thick tin-base. *Adv. Tribol.* 915–919 (2009).
3. Zhu, L. L., Wu, X. H., Zhao, G. Q. & Wang, X. B. Tribological characteristics of bisphenol S bis(diphenyl phosphate) as a high-performance antiwear additive in lubricating greases at elevated temperature. *Lubr. Sci.* **28**, 433–448 (2016).
4. Kimura, Y., Wakabayashi, T., Okada, K., Wada, T. & Nishikawa, H. Boron nitride as a lubricant additive. *Wear* **232**, 199–206 (1999).
5. Wang, S. L. & Ramaekers, J. A. H. Measurement of friction and material flow-stress by a plane-strain compression tribometer. *J. Mater. Process. Technol.* **57**, 345–350 (1996).
6. Sun, L., Zhang, C. H., Li, J. J., Liu, Y. H. & Luo, J. B. Superlubricity of Si<sub>3</sub>N<sub>4</sub> sliding against SiO<sub>2</sub> under linear contact conditions in phosphoric acid solutions. *Sci. China Technol. Sci.* **56**, 1678–1684 (2013).
7. Lin, C.-H. et al. A flexible solar-blind 2D boron nitride nanopaper-based photo-detector with high thermal resistance. *NPJ 2D Mater. Appl.* **2**, 23 (2018).
8. Woods, C. R. et al. Commensurate-incommensurate transition in graphene on hexagonal boron nitride. *Nat. Phys.* **10**, 451–456 (2014).
9. Li, L. H. & Chen, Y. Atomically thin boron nitride: unique properties and applications. *Adv. Funct. Mater.* **26**, 2594–2608 (2016).
10. Laturia, A., Van de Put, M. L. & Vandenberghe, W. G. Dielectric properties of hexagonal boron nitride and transition metal dichalcogenides: from monolayer to bulk. *NPJ 2D Mater. Appl.* **2**, 6 (2018).
11. Li, L. H. et al. Dielectric screening in atomically thin boron nitride nanosheets. *Nano Lett.* **15**, 218–223 (2015).
12. Lončarić, I., Rukelji, Z., Silkin, V. M. & Despoja, V. Strong two-dimensional plasmon in Li-intercalated hexagonal boron-nitride film with low damping. *NPJ 2D Mater. Appl.* **2**, 33 (2018).
13. Li, J. J., Zhang, C. H., Deng, M. M. & Luo, J. B. Superlubricity of silicone oil achieved between two surfaces by running-in with acid solution. *RSC Adv.* **5**, 30861–30868 (2015).
14. Li, L. H., Cervenka, J., Watanabe, K., Taniguchi, T. & Chen, Y. Strong oxidation resistance of atomically thin boron nitride nanosheets. *ACS Nano* **8**, 1457–1462 (2014).



15. Fan, D. L. et al. Hexagonal boron nitride nanosheets exfoliated by sodium hypochlorite ball mill and their potential application in catalysis. *Ceram. Int.* **42**, 7155–7163 (2016).
16. Bai, Y. et al. Ball milling of hexagonal boron nitride microflakes in ammonia fluoride solution gives fluorinated nanosheets that serve as effective water-dispersible lubricant additives. *ACS Appl. Nano Mater.* **2**, 3187–3195 (2019).
17. Mateti, S. et al. Biocompatibility of boron nitride nanosheets. *Nano Res.* **11**, 334–342 (2017).
18. Merlo, A., Mokkaapati, V., Pandit, S. & Mijakovic, I. Boron nitride nanomaterials: biocompatibility and bio-applications. *Biomater. Sci.* **6**, 2298–2311 (2018).
19. Ciofani, G., Danti, S., Genchi, G. G., Mazzolai, B. & Mattoli, V. Boron nitride nanotubes: biocompatibility and potential spill-over in nanomedicine. *Small* **9**, 1672–1685 (2013).
20. Kumari, S. et al. Alkyl-chain-grafted hexagonal boron nitride nanoplatelets as oil-dispersible additives for friction and wear reduction. *ACS Appl. Mater. Interfaces* **7**, 3708–3716 (2015).
21. Chen, S. et al. Simultaneous production and functionalization of boron nitride nanosheets by sugar-assisted mechanochemical exfoliation. *Adv. Mater.* **31**, e1804810 (2019).
22. Guo, H. B., Qi, Y. & Li, X. D. Predicting the hydrogen pressure to achieve ultralow friction at diamond and diamondlike carbon surfaces from first principles. *Appl. Phys. Lett.* **92**, 241921 (2008).
23. Car, A., Stropnik, C., Yave, W. & Peinemann, K. V. Pebax (R)/polyethylene glycol blend thin film composite membranes for CO<sub>2</sub> separation: performance with mixed gases. *Sep. Purif. Technol.* **62**, 110–117 (2008).
24. Hoffendahl, C., Fontaine, G. & Bourbigot, S. Flame retardancy of bio-based polyether-block-amide polymer (PEBAX). *Polym. Degrad. Stab.* **98**, 1247–1255 (2013).
25. Gao, D. W. et al. Membrane fouling in an anaerobic membrane bioreactor: differences in relative abundance of bacterial species in the membrane foulant layer and in suspension. *J. Membr. Sci.* **364**, 331–338 (2010).
26. Lin, Y., Williams, T. V. & Connell, J. W. Soluble, exfoliated hexagonal boron nitride nanosheets. *J. Phys. Chem. Lett.* **1**, 277–283 (2010).
27. Geick, R., Perry, C. H. & Rupprecht, G. Normal modes in hexagonal boron nitride. *Phys. Rev.* **146**, 543–547 (1966).
28. Liu, J. J. et al. Hexagonal boron nitride nanosheets as high-performance binder-free fire-resistant wood coatings. *Small* **13**, 1602456 (2017).
29. Sainsbury, T. et al. Oxygen radical functionalization of boron nitride nanosheets. *J. Am. Chem. Soc.* **134**, 18758–18771 (2012).
30. Kim, K. S. et al. Hydrogen-catalyzed, pilot-scale production of small-diameter boron nitride nanotubes and their macroscopic assemblies. *ACS Nano* **8**, 6211–6220 (2014).
31. Weng, Q. H. et al. Highly water-soluble, porous, and biocompatible boron nitrides for anticancer drug delivery. *ACS Nano* **8**, 6123–6130 (2014).
32. Hayashi, K. et al. Tribochemical reaction dynamics simulation of hydrogen on a diamond-like carbon surface based on tight-binding quantum chemical molecular dynamics. *J. Phys. Chem. C.* **115**, 22981–22986 (2011).
33. Du, M. et al. One-step exfoliation and fluorination of boron nitride nanosheets and a study of their magnetic properties. *Angew. Chem. Int. Ed.* **126**, 3719–3723 (2014).
34. Chang, B. P., Akil, H. M., Affendy, M. G., Khan, A. & Nasir, R. B. M. Comparative study of wear performance of particulate and fiber-reinforced nano-ZnO/ultra-high molecular weight polyethylene hybrid composites using response surface methodology. *Mater. Des.* **63**, 805–819 (2014).
35. Li, X. Q. et al. Effect of h-BN content on the friction and wear characteristics of B<sub>4</sub>C-h-BN ceramic composites under dry sliding condition. *Ceram. Int.* **41**, 3918–3926 (2015).
36. Cho, D. H., Kim, J. S., Kwon, S. H., Lee, C. & Lee, Y. Z. Evaluation of hexagonal boron nitride nano-sheets as a lubricant additive in water. *Wear* **302**, 981–986 (2013).
37. Chen, X. et al. Evolution of tribo-induced interfacial nanostructures governing superlubricity in a-C:H and a-C:H:Si films. *Nat. Commun.* **8**, 1675 (2017).
38. Balcombe, R., Fowell, M. T., Olver, A. V., Ioannides, S. & Dini, D. A coupled approach for rolling contact fatigue cracks in the hydrodynamic lubrication regime: the importance of fluid/solid interactions. *Wear* **271**, 720–733 (2011).
39. Cao, Z. Y., Zhao, W. W. & Zhang, J. Y. Super-elasticity and ultralow friction of hydrogenated fullerene-like carbon films: associated with the size of graphene sheets. *Adv. Mater. Interfaces* **5**, 1701303 (2018).
40. Wang, C. B., Yang, S. R., Wang, Q., Wang, Z. & Zhang, J. Y. Super-low friction and super-elastic hydrogenated carbon films originated from a unique fullerene-like nanostructure. *Nanotechnology* **19**, 225709 (2008).
41. Lee, K. et al. Understanding the role of nanoparticles in nano-oil lubrication. *Tribol. Lett.* **35**, 127–131 (2009).
42. Tong, B. H., Wang, G. Y. & Sun, X. Q. Investigation of the fluid-solid thermal coupling for rolling bearing under oil-air lubrication. *Adv. Mech. Eng.* **7**, 835036 (2015).
43. Wen, S. & Huang, P. *Principles of Tribology*. 4th ed. (Tsinghua University Press, China, 2012).
44. Belozerova, E. P. Effect of plastic deformation, produced by high-frequency vibrations, on the internal friction and young's modulus of alkali-halide crystals. *Sov. Phys. Solid State* **5**, 1480–1481 (1964).
45. Bowden, F. P. Adhesion and friction. *Endeavour* **16**, 5–18 (1957).
46. Erdemir, A. & Donnet, C. Tribology of diamond-like carbon films: recent progress and future prospects. *J. Phys. D: Appl. Phys.* **39**, R311–R327 (2006).
47. Zilibotti, G., Righi, M. C. & Ferrario, M. Ab initio study on the surface chemistry and nanotribological properties of passivated diamond surfaces. *Phys. Rev. B.* **79**, 075420 (2009).
48. Kondyurin, A., Volodin, P. & Weber, J. Plasma immersion ion implantation of Pebax polymer. *Nucl. Instrum. Methods Phys. Res., Sect. B.* **251**, 407–412 (2006).



**Open Access** This article is licensed under a Creative Commons Attribution 4.0 International License, which permits use, sharing, adaptation, distribution and reproduction in any medium or format, as long as you give appropriate credit to the original author(s) and the source, provide a link to the Creative Commons license, and indicate if changes were made. The images or other third party material in this article are included in the article's Creative Commons license, unless indicated otherwise in a credit line to the material. If material is not included in the article's Creative Commons license and your intended use is not permitted by statutory regulation or exceeds the permitted use, you will need to obtain permission directly from the copyright holder. To view a copy of this license, visit <http://creativecommons.org/licenses/by/4.0/>.

© The Author(s) 2019